Whole rock chemistry of S-type leucogranites in far-eastern Nepal

Takeshi IMAYAMA

Research Institute of Natural Sciences,
Okayama University of Science,
1-1 Ridai-cho, Kita-ku, Okayama 700-0005, Japan

Whole rock chemistry from thirteen leucogranite samples in far-eastern Nepal shows peraluminous compositions and low CaO contents, indicating that they are S-type granites. These leucogranites are subdivided into two-mica, tourmaline-bearing, and garnet-bearing leucogranites. Two-mica leucogranites are characterized by higher Sr and Ba contents and lower Rb/Sr ratio against Sr content, compared to tourmaline-bearing leucogranites. The difference might be explained by different melting temperature from same source: two-mica leucogranites crystallized from hotter magma than tourmaline-bearing leucogranites. Garnet-bearing leucogranites were characterized by low TiO_2 and CaO contents and high K_2O/Na_2O and Ba/Zr ratios, resulting from the decreasing of biotite and the increasing of K-feldspar by biotite dehydration reaction of biotite + plagioclase + sillimanite + quartz = garnet + K-feldspar + melt. The unzoned garnets in leucogranites, in contrast to a retrograded garnet zoning in the surrounding migmatites, also support that garnets in leucogranite grew as peritectic phase equilibrated with melt, rather than they were entrapped as restite garnets from metasediments.

Keyword: whole rock chemistry; S-type granite; Himalaya; Nepal.

1. Introduction

Cenozoic magmatism and metamorphism occurred in the Himalaya orogen which formed by ca. 50 Ma Indian-Asian collisions. The Himalayan leucogranites have been assigned as the S-type leucogranites (e.g., Le Fort, 1975), and they were generally produced in Early Miocene (e.g., Searle et al. 2010 and references therein). Fluid-fluxed melting (Le Fort et al., 1987; Prince et al., 2001), muscovite dehydration melting (Inger and Harris et al., 1993; Imayama et al., 2010, 2012), and biotite dehydration melting (Groppo et al., 2012) have been suggested as the mechanisms for production of the leucogranites. Main types of leucogranites are two-mica leucogranites and tourmaline-bearing leucogranites. The two-type leucogranites are considered as the results from 1) fractional crystallization (Scaillet et al., 1990), 2) different source from different protolith (Guillot and LeFort, 1995), and 3) different melting temperature from a source (Harris et al., 1993; Scaillet et al., 1995). Garnet-bearing leucogranites have been also found in the Himalaya, and there is a discussion about the origin of garnets whether new growth by melting reaction such as biotite dehydration reaction (i.e., peritectic garnet) or entrainment of relict garnets originally derived from metasedimentary source (Taylor and Stevens, 2010; Bartoli et al., 2013). In far-eastern Nepal, the S-type leucogranites have been well-known (Imayama et al., 2010, 2012; Imayama and Suzuki, 2013), but the petrogenesis of the leucogranites still remains uncertain. Therefore, in this study, whole rock and mineral chemistry of the S-type leucogranites in far-eastern Nepal were analyzed to understand the igneous petrogenesis.
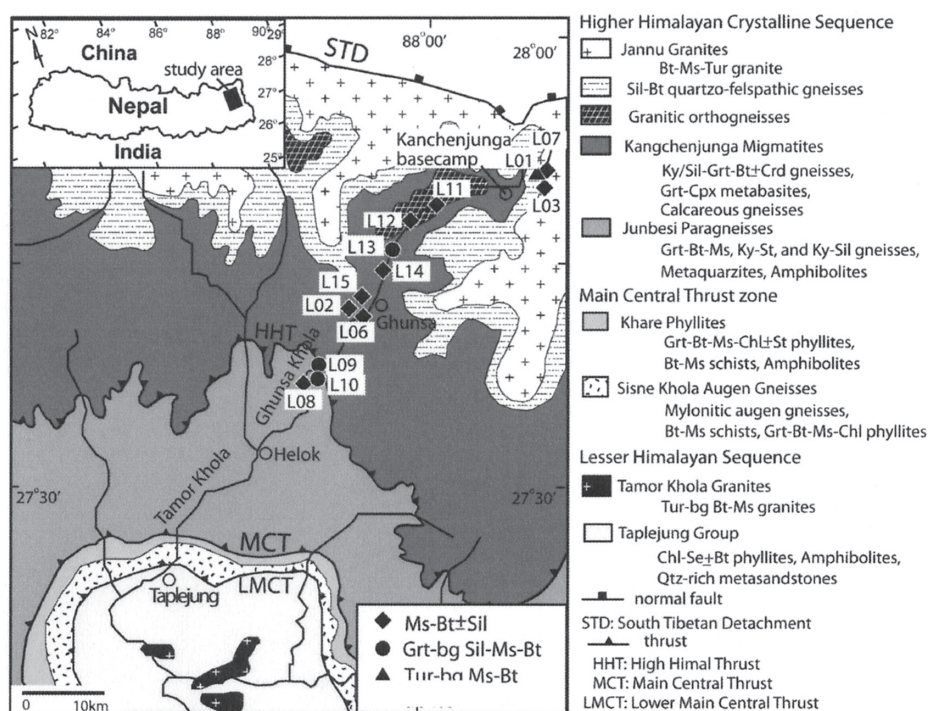
Fig. 1 Geological map along the Tamor-Ghunsa transect in far-eastern Nepal (after Imayama et al., 2010), showing locations of samples used for whole-rock analyses. Bt: biotite; Ms: muscovite; Tur: tourmaline; Grt: garnet; Sil: sillimanite; Ky: kyanite; Crd: cordierite; Cpx: clinopyroxene; Chl: chlorite; St: staurolite; Qtz: quartz; Kfs: K-feldspar.

2. Geological setting and sample descriptions

The High Himalayan Crystalline Sequence (HHCS) in far-eastern Nepal are mainly composed of leucogranites, amphibolite to granulite facies gneisses, and migmatites (Fig. 1: Goscombe et al. 2006; Imayama et al. 2010, 2012). The HHCS overlies the Lesser Himalayan Sequence consisting of low-grade metasediments along the Main Central Thrust (MCT). The Tamor-Ghunsa section is located at the foot of Mt. Kanchenjunga in far-eastern Nepal. The leucogranites occur as sills and dykes in the HHCS. Imayama and Suzuki (2013) reported that melt crystallization occurred at 21-18 Ma based on CHIME monazite dating. Two-stage partial melting has been recognized in this area, which is shown by 21–18 Ma migmatite at the middle HHCS and 31–27 Ma migmatite at the upper HHCS (Imayama et al., 2012). The Early Oligocene migmatites has been intruded by Early Miocene leucogranites.

For whole rock chemistry, thirteen leucogranite samples were collected from the HHCS along Tamor-Ghunsa section (Fig. 1). These leucogranites are white color in appearance, and they are classified into three groups on the basis of mineral assemblages: two-mica leucogranites (samples L02–03, L06–08, L11–12, and L14–15), tourmaline-bearing leucogranites (sample L01), and garnet-bearing leucogranites (samples L09–10 and L13). Two-mica leucogranites are composed of quartz, plagioclase, K-feldspar, muscovite, biotite ± sillimanite (Fig. 2a) with accessory minerals of apatite, monazite, zircon, and xenotime. Biotites partly show alteration to chlorites. A lot of feldspars are found in samples L06–07, L11–12, and L14. Tourmaline-bearing leucogranite, which was corrected from the floats at the Kanchenjunga basecamp, consists of biotite, muscovite, tourmaline, plagioclase, quartz, and K-feldspar (Fig. 2b). Euhedral tourmalines are 1 to 10 mm in length. Garnet-bearing leucogranites contain quartz, plagioclase, K-feldspar, sillimanite, garnet, muscovite, and biotite (Fig. 2c) with accessory minerals of apatite, monazite, and zircon. Garnets range in size from 0.5 to 5 mm. They are often broken and are partly replaced by biotite and chlorite along the fractures.
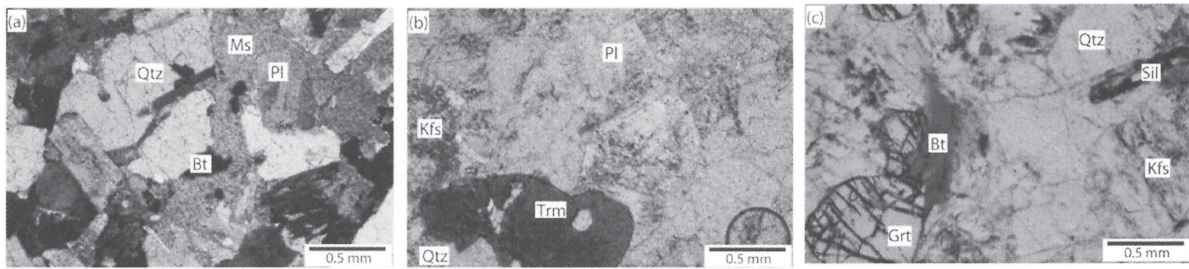
Fig. 2. Photographs of (a) two-mica leucogranite (sample L06), (b) tourmaline-bearing leucogranite (sample L01), and (c) garnet-bearing leucogranite (sample L09). Pl: plagioclase. Same abbreviations are used in Fig. 1.

3. Whole-rock compositions

Whole-rock compositions were analyzed using a SHIMADZU XRF1800 wavelength dispersive sequential X-ray fluorescence spectrometer with an end-window 4kW Rh X-ray tube at Nagoya University. 100 to 200 g samples were first crushed on a cast iron plate by pounding with a hammer, and powdered using an agate mortar. After drying in an oven heated to 110 °C for 24 hours, they were mixed with anhydrous lithium tetraborate (0.7 g sample and 6 g flux for analysis of major elements and 2 g sample and 3 g flux for trace elements) and fused with a Pt90Au10 crucible in an electric furnace to make the glass bead. The tube voltage was 40 kV, and the tube current was 70 mA for major elements and 95 mA for the trace elements. The detection limits were 10 ppm for Ba and 0.5–2 ppm for other trace elements at the 2σ confidence level. The results of XRF analyses for leucogranites are listed in Table 1.

All leucogranites are peraluminous with Al_2O_3/ $(CaO+Na_2O+K_2O)$ ratios (molar) of 1.1–1.9 (Fig. 3a), which are characteristics of the S-type granites. Garnet-bearing leucogranites especially show high Al_2O_3/ $(CaO+Na_2O+K_2O)$ ratios. This is because garnet is highly aluminous as well as muscovite in phases of granite. The SiO_2 contents range from 71.2 to 77.4 wt %. The TiO_2 (0.01–0.07 wt. %) contents of tourmaline-bearing and garnet-bearing leucogranites show relatively lower values than those (0.09–0.45 wt. %) of two-mica leucogranites (Fig. 3b), indicating a low amount of biotite. The CaO (0.41–2.71 wt. %) contents are generally low (Fig. 3c), compared to those in the I-type leucogranites. The CaO contents and K_2O/Na_2O ratios are negatively correlated. Garnet-bearing leucogranites have higher K_2O/Na_2O ratios and lower CaO contents, compared to the other leucogranites (Fig. 3c), probably reflecting a low amount of plagioclase. In contrast, the increase in Ba/Zr ratios are clearly associated with increasing K_2O/Na_2O ratios (Fig. 3d), resulting from a large number of K-feldspar in garnet-bearing leucogranites. Total alkalis vary from 1.2–10.4 wt. % (Table 1), and there is negative correlation between K_2O and Na_2O. Zirconium contents are 29–265 ppm. Tourmaline-bearing leucogranites are characterized by low Sr and Ba contents, compared to those of the other leucogranites (Fig. 3e). Tourmaline-bearing and garnet-bearing leucogranites represent highest and lowest Rb/Sr ratios against Sr content, respectively (Fig. 3f).
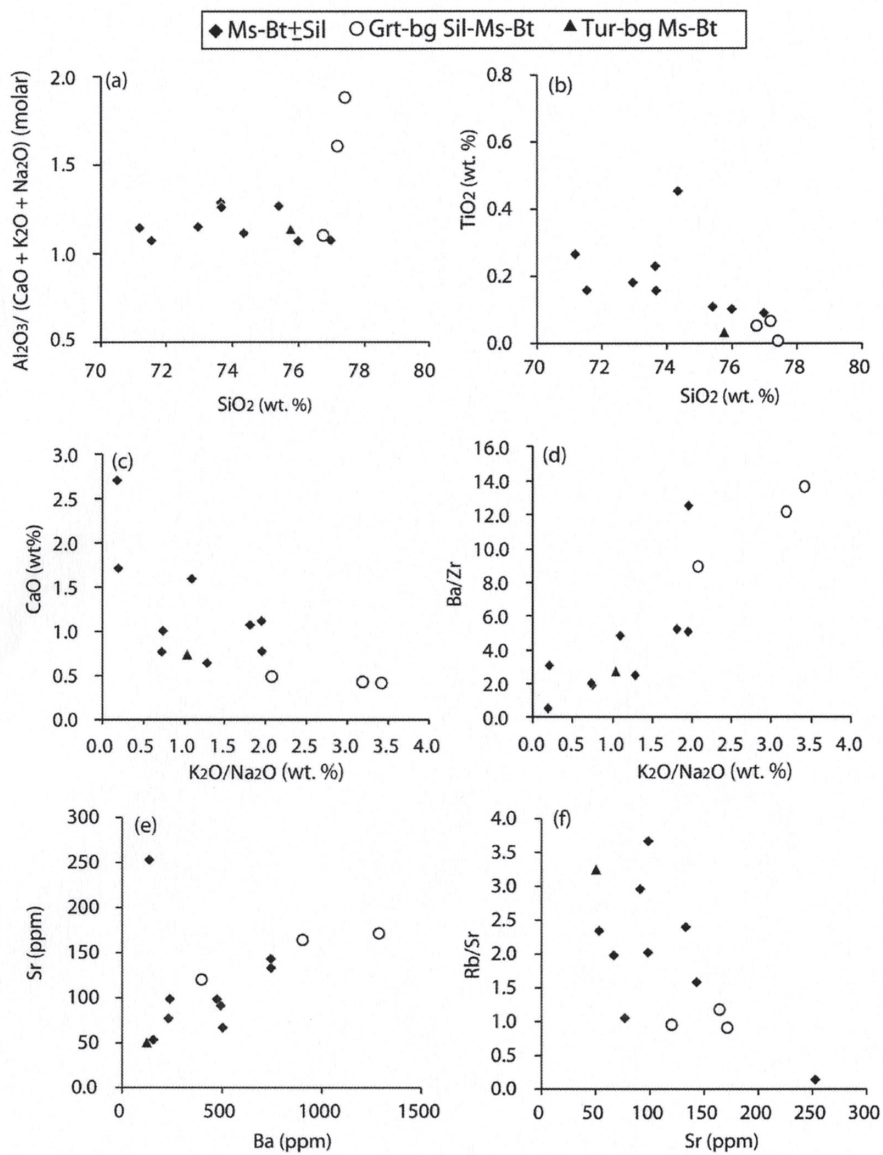
Fig. 3 Whole rock compositions from leucogranites. (a) alumina saturation and (b) TiO_2 content against SiO_2 content. (c) CaO content and (d) Ba/Zr against K_2O/Na_2O. (e) Sr versus Ba contents. (f) Rb/Sr versus Sr content.

Table 1 XRF analyses of leucogranites, far-eastern Nepal

Samples	L01	L02	L03	L06	L07	L08	L09
Major elements (wt. %)							
SiO_2	75.76	71.18	75.40	74.34	76.98	75.99	77.18
TiO_2	0.03	0.27	0.11	0.45	0.09	0.10	0.066
Al_2O_3	14.82	16.19	14.99	12.58	12.24	15.02	14.46
Fe_2O_3	0.51	1.93	0.90	2.37	1.02	0.54	1.26
MnO	0.01	0.02	0.02	0.03	0.02	0.01	0.05
MgO	0.12	0.46	0.14	0.73	0.23	0.20	0.21
CaO	0.74	1.71	0.77	1.00	0.76	2.71	0.42
Na_2O	4.22	5.93	2.77	3.87	4.12	4.95	1.62
K_2O	4.37	1.18	5.41	2.87	3.00	0.91	5.14
P_2O_5	0.07	0.14	0.07	0.09	0.12	0.07	0.09
Total	100.65	99.02	100.58	98.32	98.58	100.50	100.49
Trace elements (ppm)							
Th	8.8	92.8	8.4	37.2	12.0	1.1	8.4
Pb	59.1	51.0	74.5	23.4	43.7	48.2	71.9
Ba	123.0	231.4	492.8	503.1	155.2	135.2	1287.3
Nb	nd	0.7	nd	nd	nd	nd	nd
Zr	44.8	75.6	39.3	265.8	77.0	256.2	105.8
Y	19.6	248.5	13.6	51.1	48.6	5.4	17.7
Sr	50.5	76.9	91.1	66.8	53.3	252.8	171.3
Rb	164.1	81.0	269.5	132.0	124.8	35.8	155.8
As	Nd	nd	8.0	nd	0.0	36.4	43.2
Zn	7.1	46.8	17.9	21.1	15.8	12.2	11.2
Cu	nd	nd	nd	nd	nd	nd	nd
Ni	4.2	6.5	3.4	8.3	4.2	5.8	5.8
Co	nd	4.0	0.5	5.7	0.7	0.0	1.3
Cr	13.7	4.6	18.4	86.9	0.7	19.7	14.5
V	1.3	6.3	5.0	35.0	1.8	8.4	15.8

Samples	L10	L11	L12	L13	L14	L15
Major elements (wt. %)						
SiO_2	77.41	73.64	71.54	76.75	73.66	72.95
TiO_2	0.01	0.23	0.16	0.05	0.16	0.18
Al_2O_3	15.02	15.78	16.35	13.09	15.12	15.12
Fe_2O_3	0.50	1.50	0.79	0.67	1.44	0.97
MnO	0.04	0.03	0.02	0.02	0.04	0.02
MgO	0.02	0.33	0.14	0.09	0.24	0.28
CaO	0.41	1.59	1.11	0.48	0.64	1.07
Na_2O	1.35	3.31	3.53	2.83	3.58	3.11
K_2O	4.62	3.61	6.86	5.86	4.58	5.62
P_2O_5	0.13	0.06	0.11	0.04	0.18	0.16
Total	99.51	100.08	100.61	99.88	99.64	99.48
Trace elements (ppm)						
Th	nd	8.4	19.6	16.8	6.4	19.8
Pb	52.7	74.5	68.3	94.9	63.8	70.9
Ba	397.1	492.8	745.4	903.5	238.1	743.9
Nb	nd	nd	nd	nd	nd	nd
Zr	29.1	39.3	147.0	101.2	95.7	142.3
Y	5.5	13.6	16.2	21.9	20.7	16.3
Sr	120.1	91.1	133.0	164.2	98.5	143.0
Rb	114.7	269.5	319.1	193.5	361.3	226.2
As	37.4	8.0	35.1	45.7	48.4	41.4
Zn	nd	17.9	16.1	4.0	31.6	20.0
Cu	nd	nd	nd	3.0	nd	nd
Ni	4.2	3.4	4.3	3.7	4.1	6.4
Co	nd	0.5	0.1	nd	1.7	0.6
Cr	15.9	18.4	11.0	9.5	13.7	23.7
V	4.2	5.0	11.7	7.0	13.1	14.3

nd = not detected

4. Mineral compositions

Garnet and biotite compositions from garnet-bearing leucogranite were analyzed using a Cameca SX-51 electron-probe microanalyzer at the Jeonju branch of the Korea Basic Science Institute, South Korea. They operated with a 15 kV accelerating voltage and 20 nA beam current.

Garnets in sample L09 show a homogenous composition with no zonation, and it yields almandine-rich and grossular-poor composition ($Alm_{76-77}Pyp_{15-16}Sps_{5-6}Grs_2$). The Fe/ (Fe + Mg) ratio (X_{Fe}) is 0.83–0.84. The biotite inclusions in the garnets have X_{Fe} ratio of 0.47–0.49, whereas the biotite grains in the matrix have higher X_{Fe} ratio (ca. 0.58).

5. Discussion

The characters of the S-type granite in far-eastern Nepal were confirmed by peralminous compositions and low CaO contents. Generally, two-mica leucogranites from the other areas in Nepal show relatively higher TiO_2, CaO, and Ba contents and lower Rb/Sr ratio against Sr content, compared to tourmaline-bearing leucogranites (Scaillet et al., 1990, 1995; Harris et al., 1993; Guillot and Le Fort, 1995). In far-eastern Nepal, as well as the other areas, two-mica leucogranites yield the relatively higher TiO_2 and Ba contents and lower Rb/Sr ratio against Sr content, compared to tourmaline-bearing leucogranite. With respect to the CaO content, the difference between two-mica and tourmaline-bearing leucogranites is unclear, probably due to the low number of tourmaline-bearing leucogranite sample.

Scaillet et al. (1990) suggested that two-mica leucogranites can be formed by fractional crystallization of tourmaline-bearing leucogranites. They reported that CaO content in bulk rock is negatively correlated to Na_2O and Rb, whereas it is positively correlated with K_2O, TiO_2, Sr, Ba, and Zr. However, in this study, such a trend is not observed. Guillot and Le Fort (1995) proposed different magma sources between them: tourmaline-bearing leucogranite is a metagreywacke origin, whereas two-mica leucogranite is a metapelitic origin. In far-eastern Nepal, the pelites and metagreywacke in the HHCS are often alternated. Therefore, it seems to be difficult to form separately different magmas from pelites and metagreywacke. As alternative model, Harris et al. (1993) proposed that different melting temperature from same source can form two-type granites: two mica leucogranite crystallized directly from higher temperature melts (i.e., a high-degree primary melt) than tourmaline-bearing leucogranites represented by a low-degree primary melt. In this area, two-mica leucogranites are abundant in contrast to minor tourmaline-bearing leucogranites. This may be attributed to the high metamorphic grade (700–820 °C) and prolonged high-temperature metamorphism in this area (Imayama et al., 2012; Ambrose et al., 2015). Therefore, the model explained by different melting temperature from a source could be preferred.

According to Imayama et al. (2010, 2012), the existence of muscovite-out isograd and the P–T conditions of migmatites indicate that most leucogranites in far-eastern Nepal were produced by fluid-absent muscovite dehydration reaction of muscovite + plagioclase + quartz = aluminosilicate + K-feldspar + melt (Imayama et al. 2012). In addition, the existence of garnet in leucogranite implies that the biotite dehydration reaction of biotite + plagioclase + sillimanite + quartz = garnet + K-feldspar + melt also occurred. The low TiO_2 and CaO contents and high K_2O/Na_2O and Ba/Zr ratios in garnet-bearing leucogranites represent the decreasing of biotite and the increasing of K-feldspar, which is matched with the assumption that biotite dehydration reaction proceeded. Alternatively, garnet in leucogranite could be entrapped from the metasediments when partial melting occurred. However, unzoned garnet in garnet-bearing leucogranites is different from retrograde garnet zoning with Mn and Fe-rich garnet rims from the migmatites in this area (e.g., Imayama et al., 2010). Also, metamorphic temperature from the middle and upper HHCS in far-eastern Nepal is enough high (700–820 °C, Imayama et al., 2010) to occur the biotite dehydration reaction (Le Breton and Thompson, 1988). These observations support that garnets in leucogranite grew as a peritectic phase equilibrated with melt, rather than entrainment of restite garnets from metasediments.

Reference

Ambrose, T. K., Larson, K. P., Guilmette, C., Cottle, J. M., Buckingham, H., and Rai, S., 2015. Lateral extrusion, underplating, and out-of-sequence thrusting within the Himalayan metamorphic core, Kanchenjunga, Nepal. Lithosphere, v. 7, p. 441–464.

Bartoli, O., Tajčmanová, L., Cesre, B., and Acosta-Vigil, A., 2013. Phase equilibria constraints on melting of stromatic migmatites from Ronda (S. Spain): insights on the formation of peritectic garnet. Journal of Metamorphic Geology, v. 31, p. 775–789.

Goscombe, B., Gray, D., and Hand, M., 2006. Crustal architecture of the Himalayan metamorphic front in eastern Nepal. Gondwana Research, 10: 232-255.

Groppo, C., Rolfo, F., and Indares, A., 2012. Partial melting in the Higher Himalayan Crystallines of eastern Nepal: the effect of decompression and implications for the 'channel flow' model. Journal of Petrology, v. 53, p. 1057–1088.

Guillot, S., and Le Fort, P., 1995. Geochemical constrains on the bimodal origin of High Himalayan leucogranites. Lithos, 35, 221–234.

Harris, N., Inger, S., and Massey, J., 1993. The role of fluids in the formation of High Himalayan leucogranites. In: Treloar, P. J., and Searle, M. P. (eds) Himalayan Tectonics. Geological Society, London, Special Publication, v. 74, p. 391–400.

Imayama, T., Takeshita, T., and Arita, K., 2010. Metamorphic P–T profile and P–T path discontinuity across the far-eastern Nepal Himalaya: investigation of channel flow models. Journal of Metamorphic Geology, v. 28, p. 527–549.

Imayama, T., Takeshita, T., Yi, K, Cho, D. –L., Kiatajima, K., Tsutsumi, Y., Kayama, M., Nishido, H., Okumura, T., Yagi, K., Itaya, T., and Sano, Y., 2012. Two-stage partial melting and contrasting cooling history within the Higher Himalayan Crystalline Sequence in the far-eastern Nepal Himalaya. Lithos, v. 134-135, p. 1–22.

Imayama, T., and Suzuki, K., 2013. Carboniferous inherited grain and age zoning of monazite and xenotime from leucogranites in far-eastern Nepal: constraints from electron probe microanalysis. American Mineralogist, v. 98, p. 1393–1406.

Inger, S., and Harris, N., 1993. Geochemical constraints on leucogranite magmatism in the Langtang Valley, Nepal Himalaya. Journal of Petrology, v. 3, p. 345–368.

Le Breton, N., and Thompson, A. B., 1988. Fluid-absent (dehydration) melting of biotite in metapelites in early stages of crustal anatexis. Contributions to Mineral and Petrology, v. 99, p. 226–237.

Le Fort, P., 1975. Himalayas: The collided range. Present knowledge of the continental arc. American Journal of Science, v. 275A, p. 1–44.

Le Fort, P., Cuney, M., Deniel, C., France-Lanord, C., Sheppard, S. M. F., Upreti, B. N., and Vidal, P., 1987. Crustal generation of Himalayan leucogranites. Tectonophysics, v. 134, p. 39–57.

Prince, C., Harris, N., and Vance, D., 2001. Fluid-enhanced melting during prograde metamorphism. Journal of the Geological Society, London, v. 158. p. 233–241.

Scaillet, B., France-Lanord, C., and Le Fort, P., 1990. Badrinath-Gangotri plutons (Garhwal, India): petrological and geochemical evidence for fractionation processes in a high Himalayan leucogranite. Journal Volcanology and Geothermal Research, v. 44, p. 163–188.

Scaillet, B., Pêcher, A., Rochette, P., and Champenois, M., 1995. The Gangotri granite (Garhwal Himalaya): Laccolithic emplacement in an extending collisional belt. Journal of Geophysics Research, v. 100, p. 585–607.

Searle, M. P., Cottle, J. M., Streule, M. J., and Waters, D. J., 2010. Crustal melt granites and migmatites along the Himalaya: melt source, segregation, transport and granite emplacement mechanisms. Geological Society of America Special Papers, v. 472, p. 219–233.

Taylor, J., and Stevens, G., 2010. Selective entrainment of peritectic garnet into S-type granitic magmas: Evidence from Archaean mid-crustal anatectites. Lithos, v. 120, p. 277–292.